



*Research article*

## Mechanical analysis of PDMS material using biaxial test

João E. Ribeiro<sup>1,2</sup>, Hernani Lopes<sup>3</sup>, Pedro Martins<sup>4</sup> and Manuel Braz-César<sup>1,5,\*</sup>

<sup>1</sup> School of Technology and Management, Polytechnic Institute of Bragança, Campus de Santa Apolónia, 5300-253 Bragança, Portugal

<sup>2</sup> CIMO, Campus de Santa Apolónia, 5300-253 Bragança, Portugal

<sup>3</sup> Mechanical Engineering Department, ISEP, Polytechnic Institute of Porto, Dr. António Bernardino de Almeida Street, 431, 4200-072 Porto, Portugal

<sup>4</sup> Mechanical Engineering Department, FEUP, Dr. Roberto Frias Street, 4200-465 Porto, Portugal

<sup>5</sup> CONSTRUCT-LESE, FEUP, Dr. Roberto Frias Street, 4200-465 Porto, Portugal

\* **Correspondence:** Email: [brazcesar@ipb.pt](mailto:brazcesar@ipb.pt).

**Abstract:** Polydimethylsiloxane (PDMS) materials are classified as a silicone and commonly present a hyperelastic behaviour. Many researchers have studied PDMS in recent years, motivated by its applications in the biomedical field. In the present manuscript, a biaxial tensile test performed at different speeds is described. The displacement field for the different experimental test conditions is measured using the digital image correlation technique. Numerical studies were also carried out using the most popular constitutive models, namely Mooney-Rivlin, Yeoh and Ogden, for comparison with the experimental measurements. From the experimental displacement profile taken along the central section of each sample, that this tensile test presents linear behaviour; it is an independent speed test. The same conclusion can be found from the numerical results. The results of the numerical simulation show that they are strongly dependent on the constitutive model of the material. The numerical simulations with the Yeoh model presented the most accurate results for PDMS behaviour. Another important conclusion is that the digital image correlation technique is well suited for the analysis of hyperelastic materials.

**Keywords:** hyperelasticity; polydimethylsiloxane (PDMS); experimental tests; numerical simulation; digital image correlation

---

## 1. Introduction

In recent decades, the characterization of biological tissues has had an enormous evolution [1–3]. Biomedical engineering has been at the vanguard in biological tissues study and in the development of new materials with the objective of replacing organic tissues when other therapies are not possible or not recommended. Usually, human biological tissues can be classified into soft and hard tissues [4]. Soft tissues have an extracellular matrix that is rich in collagen and elastin fibres, as in the case of connective, epithelial and muscle tissue [5]. The hard tissues have a mineralized extracellular matrix that contains calcium or enamel, the most well-known being bones and teeth [5]. These two groups of materials present completely different mechanical behaviour when submitted to external loads, requiring, for this reason, different approaches to their study. Soft tissues, in particular, are known for presenting a hyperelastic behaviour that is characterized by a high strain before reaching tensile strength [6]. The stress–strain relationship can be derived from a function of strain energy density [7], which can be linear or nonlinear and reversible.

The need for replacement of some biological tissues in severe injuries has driven the development of new artificial materials with very similar characteristics and behaviour to these natural tissues. There are many relevant applications in this particular field, such as the development of artificial skin [8] to replace the natural skin that was destroyed by the action of burns [9], artificial bone tissue [10] that can be used in patients with degenerative diseases or accidents, polypropylene mesh designed to repair human vaginal mucosa tissue [11] used in women with urinary incontinence and the application of the polydimethylsiloxane (PDMS), due to its high biocompatible, as prostheses [12–15]. PDMS, with its hyperelastic properties, could be useful for other applications, such as in lab-on-a-chip and micro- and nano-electromechanical system (MEMS/NEMS) [16,17]. These applications are examples where a deep knowledge of mechanical behaviour and the material properties of natural biological tissue was necessary.

The most appropriate approaches to characterize the behaviour of these materials, synthetic or biological, consist of two methods, experimental testing and numerical simulation. In the experimental approach, a set of tests, often with samples of the material one wants to characterize, are performed [18]. For this type of analysis laboratory facilities and very expensive equipment are necessary. However, this allows the researcher to obtain more realistic results with greater accuracy. There are several mechanical and technical measurement tests for the characterization of these tissues; the most commonly used tests are the tensile [18], fatigue [19] and creep tests. Recently, new optical full-field techniques have gained interest for characterization of the global behaviour of tissues. Laser interferometry (Moiré interferometry, electronic speckle pattern interferometry or ESPI and Shearography) [20–22] and digital image correlation (DIC) [23,24] are the most known optical techniques. On the other hand, the use of numerical approaches based on the finite element method (FEM) has been growing exponentially [25,26]. The appearance of computation tools applied to biological material was driven by lower method costs and increasing computer calculation capacity. Considering the advantages of each approach, experimental and numerical, some researchers have developed hybrid methods that use experimental information in the numerical simulations [27].

This paper aims to develop a method for the characterization of the mechanical properties of PDMS materials subjected to biaxial tensile tests. The experimental displacements and strain fields were recorded using the DIC optical technique, which allows us to more accurately identify the mechanical properties of these hyperelastic materials. Also, based on the displacements and strain

measurements, we want to identify the most suitable constitutive models that allow us to correctly simulate the behaviour of PDMS materials.

## 2. Materials and method

In the present work, a biaxial analysis of PDMS material hyperelastic behaviour was implemented. The reason for choosing a biaxial analysis applied to an isotropic material was to identify the influence of biaxial loading on the deformation field.

The experimental test consisted of applying a biaxial tensile load to the PDMS specimens and measuring the displacements and the strain fields in order to establish the relationship between the strain and the load. For this purpose, an experimental set-up was implemented to allow the performance of the biaxial tensile tests. For the measurements, it was necessary to identify a set of parameters, such as the maximum expected loads, the maximum deformations, and the implementation of a clamping system, among others. The specimens have cruciform geometry with the dimensions shown in Figure 1.

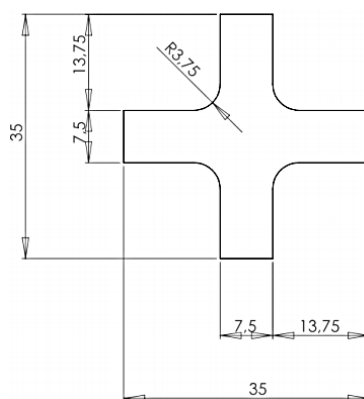


**Figure 1.** Geometry and dimensions of the tested specimens, dimensions in mm.

The test specimens were manufactured by using an aluminium alloy mould with a  $140 \times 140 \text{ mm}^2$  cavity and a 1.8 mm thickness. The cavity of the mould was filled with PDMS resin and, after the curing process, the resultant plate was cut to the geometry presented in Figure 1 using a cutting tool.

Pre-polymer PDMS and its curing agent (Sylgard 184, Dow Corning Corporation) were mixed in a 10:1 ratio to form the PDMS elastomer. After the PDMS completely cured (42 hours at room temperature), the mould was placed in an oven at 80 °C for 30 minutes. After this period, a parallelepiped  $140 \times 140 \times 1.8 \text{ mm}^3$  PDMS plate was removed from the mould, and the test specimens were extracted from each.

A random speckle pattern was artificially created on the surface of each cruciform specimen. The speckle pattern was produced using an airbrush with an internal mixture of air and paint, connected to a low-pressure compressor. First, the specimen surface was covered with white matte paint. After this, a second fine layer of small black paint dots was applied with the airbrush to produce the high-contrast speckle pattern. The size and density of the speckle were defined to guaranty high fluctuation of the image intensity, and thus, higher accuracy measurements could be obtained.

Once the random pattern was created, the sample was placed in a biaxial tensile test machine, being fixed by straps to avoid the slip between the specimen and the grips. The surface with the random speckle pattern was mounted facing the DIC system, see Figure 2.

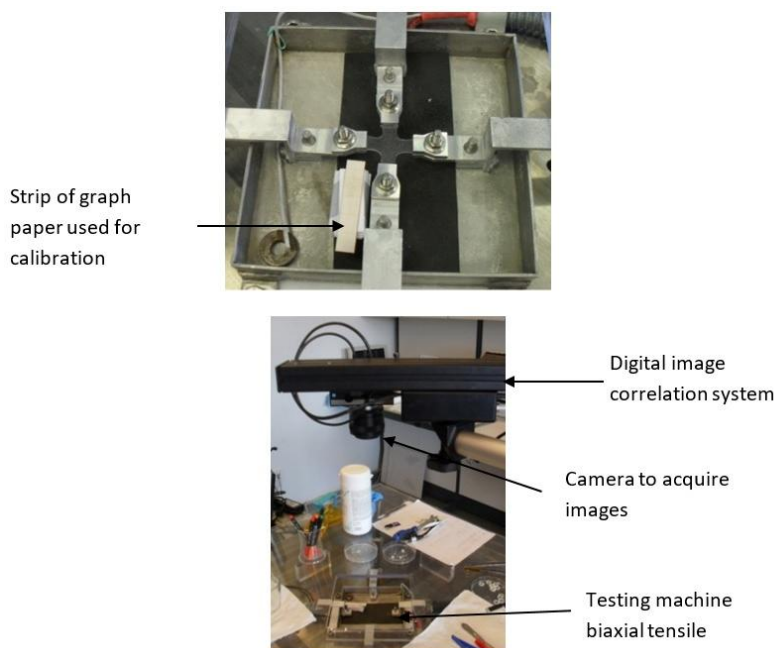


**Figure 2.** Optical assembly for performing the tensile test of PDMS using the DIC technique.

A commercial DIC system (Aramis<sup>®</sup>) with a CCD camera and a  $1624 \times 1236$  pixel resolution was used. The images were recorded and processed using the ARAMIS<sup>®</sup> software to obtain the in-plane displacement field. The DIC technique is based on a comparison between the speckle patterns of images recorded at different states of object deformation. The technique follows subregions of speckle patterns with the objective of measuring the displacement and strains produced in each loading state. To increase the effectiveness of the DIC technique, each selected pattern needs to be random and unique, with a high range of contrast levels and intensity. For this purpose, the object must be illuminated by a white light source. Normally, these subregions of speckle patterns present an equally spaced distribution along the measurement surface.

The measurement of the displacement field was held in the central region of the specimen as shown in Figure 3.

The Aramis system has two different procedures for calibration, depending on whether it will be used for 2D or 3D field measurements. For 2D field measurements, which were used in this work, the calibration procedure is simple because it only needs the definition of two points that don't move during the experimental tests and an accurate distance between them. The Aramis system includes scaling targets; however, some researchers prefer to use a standard graph paper to simplify the experimental set-up while obtaining accurate measurement results [27,28]. In the present work, the calibration of the system was performed using standard graph paper mounted close to the sample surface and defining the distance between two points. This scaling will serve as a reference for subsequently determining the displacement field on the specimen surface during the test.

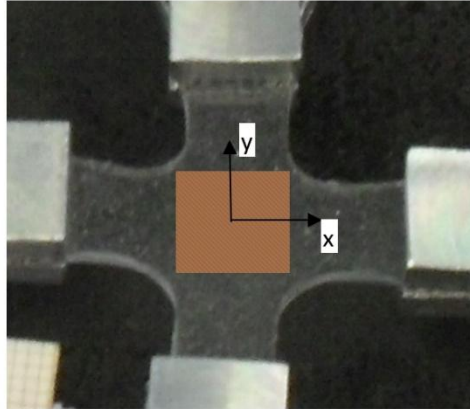


**Figure 3.** Representation of the analysed area.

PDMS specimens used in tensile tests present the geometry and dimensions shown in Figure 1 with a thickness of 1.8 mm. The biaxial tensile tests were performed with four different tensile speeds, which are presented in Table 1.

**Table 1.** Tensile test speed.

Tests	Test speed [mm/min]
1	1
2	2
3	5
4	10

The experimental test begins the unloading test by capturing of the first image, defined as the reference state, and the following images, corresponding deformation states, were captured sequentially at a constant rate of one per second. These images recorded for later post-processing using Aramis software.

### 3. Numerical simulations

The numerical simulation was implemented using a commercial finite element method (FEM) software ANSYS®.

To perform the numerical simulation, it was necessary to create a model with a geometry similar to that of the specimens and boundary conditions matching the experimental testing and to discretize the domain infinite element mesh. The loading and kinematic conditions were identical to those used in the experimental test. For the material properties, a nonlinear hyperelastic behaviour, based on the constitutive models of Mooney-Rivlin, Yeoh and Ogden, was considered. These models are recommended by many authors for the simulation PDMS materials [29,30]. The application of these models required the determination of several constants, which were identified from the experimental curves of the tensile tests.

A bi-dimensional finite-element mesh, with 12764 parametric structural solid elements (PLANE182) [31] was used and is shown in Figure 4. In relation to the boundary conditions of the numerical model, a uniform displacement was applied to the upper, bottom, left and right lips, stretching the PDMS sample. In order to validate the finite element model, simulations were carried out for different values of displacement, according to Table 2.

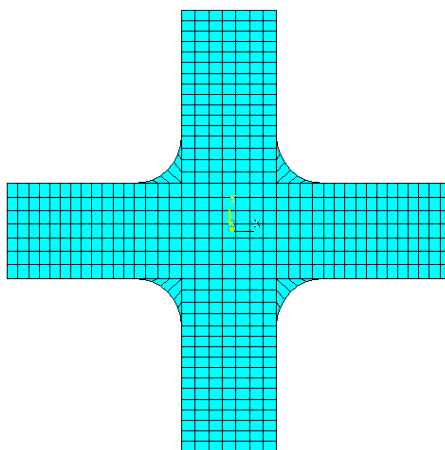


**Figure 4.** Finite element mesh used.

**Table 2.** Displacements used in numerical simulations.

Tensile speed [mm/min]	Displacement [mm]
1	1.03
2	1.50
5	1.41
10	3.32

#### 4. Results and discussion

The stress–strain curves obtained for the five test PDMS samples at different strain rates (Table 2) are shown in Figure 5a,b, respective to the X and Y directions.

PDMS typically has hyperelastic behaviour, as can be seen from the stress–strain curves plotted in Figure 5a,b. These show a very similar behaviour at high deformations, which can be a problem for other experimental techniques, such as interferometric techniques. However, DIC is one of the few optical techniques which allows the full-field measurement of displacements and strains for high deformation.

It should be noted that, although these correspond to different deformation times, the spatial distribution of the displacement field is very similar. These results prove that the DIC technique is suitable for measuring the displacement in hyperelastic material and shows that the material behaviour is independent of the strain rate applied.

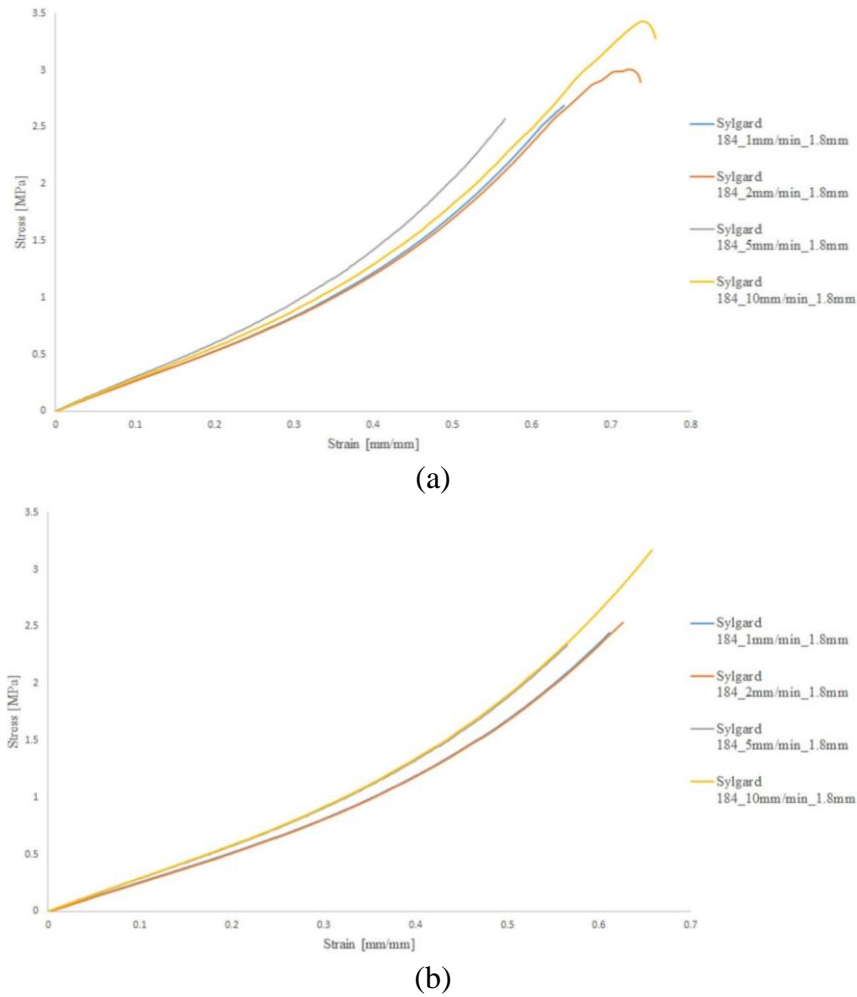


**Figure 5.** Stress–strain curves at the different strain rates (a) in the X direction and (b) in the Y direction.

The respective displacement fields in the X and Y directions, measured with the DIC technique for the minimum and maximum strain rate are shown in Figures 6 and 7, for the same displacement or strain.

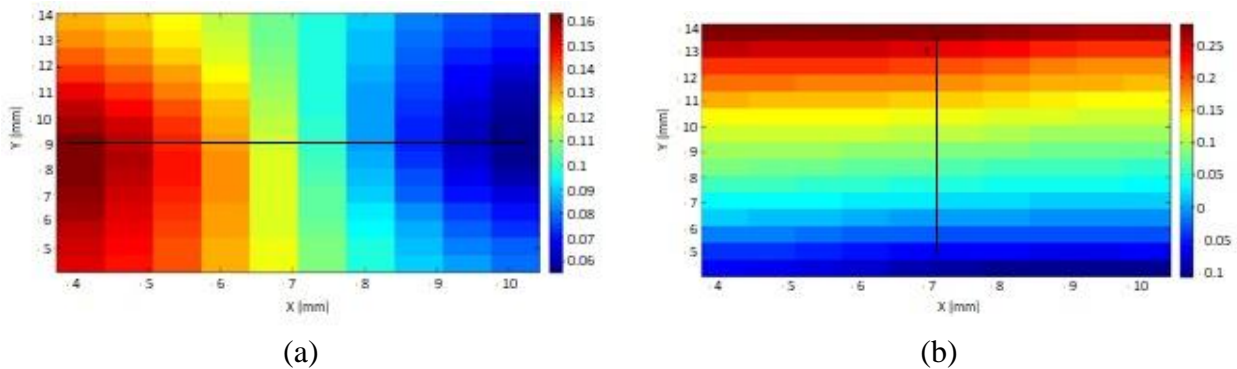


**Figure 6.** Displacement field (mm) of the specimen at a 1 mm/min strain rate using DIC (a) in the X direction and (b) in the Y direction.

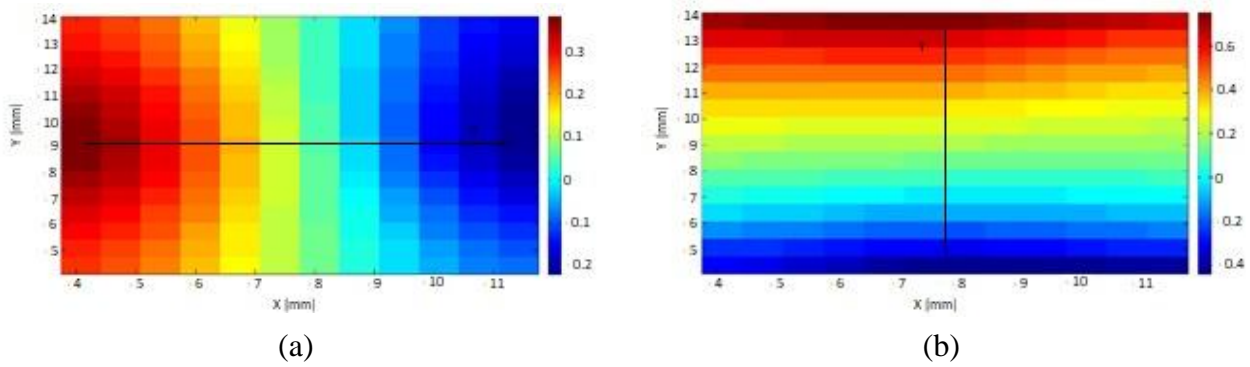


**Figure 7.** Displacement field (mm) of the specimen at a 10 mm/min strain rate using DIC (a) in the X direction and (b) in the Y direction.

As already mentioned, the displacement field is related to the central area of the specimen where its distribution is nearly linear. The profiles along the middle section, defined by black lines in Figures 6 and 7, are presented in Figures 8 and 9 for the X and Y directions.

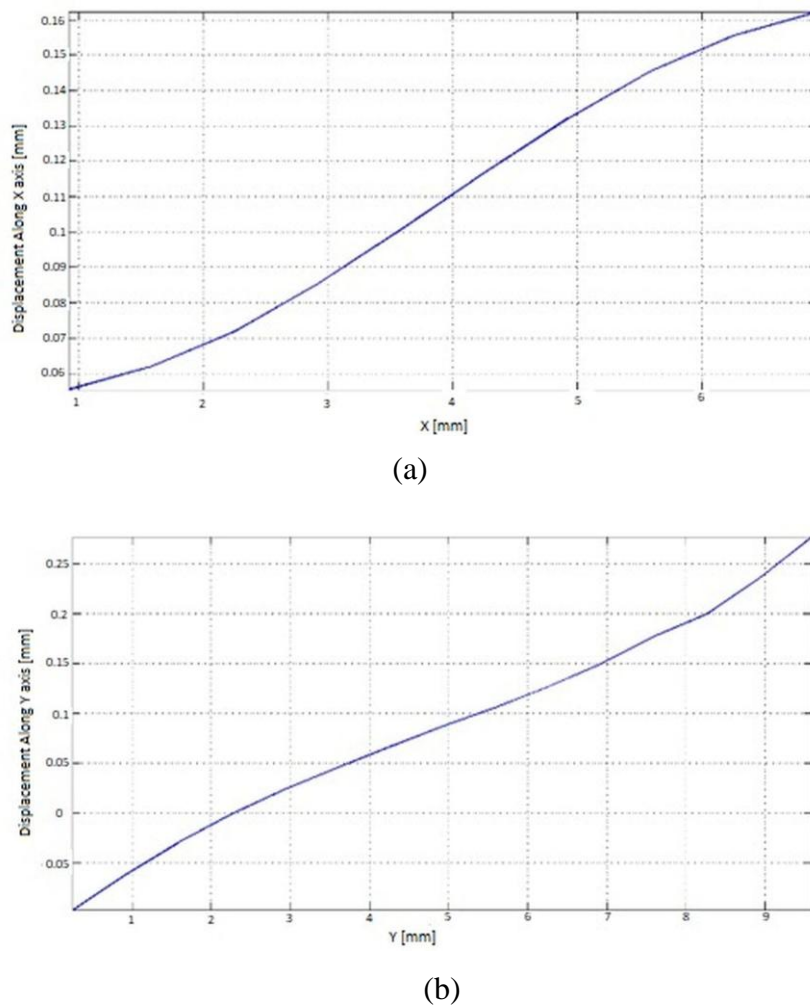
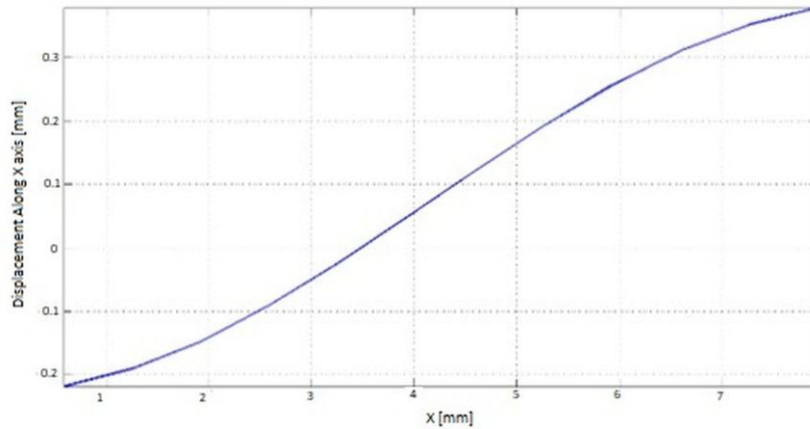
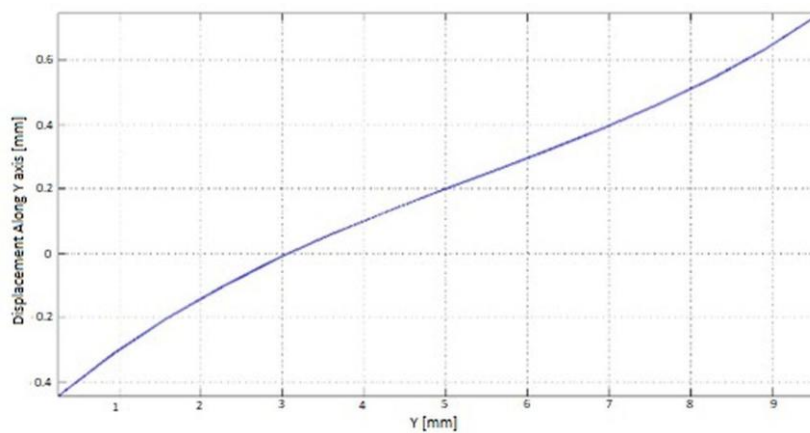


**Figure 8.** Profile of the displacement field in the central region of the specimen at a 1 mm/min strain rate using DIC (a) in the X direction and (b) in the Y direction.





(a)



(b)

**Figure 9.** Profile of the displacement field in the central region of the specimen at a 10 mm/min strain rate using DIC (a) in the X direction and (b) in the Y direction.

The analysis of the displacement distribution profile along the X and Y directions shows that they have a nearly linear distribution. These plots show different values of displacement for the same load. In Figure 8, the maximum displacement in the X direction is close to 0.16 mm, while for the Y direction, the displacement is close to 0.28 mm. In Figure 9, the displacement is 0.4 mm and 0.7 mm for the X and Y directions, respectively.

For the numerical simulation, the curves of the constitutive models of hyperelastic material, Mooney-Rivlin, Yeoh and Ogden, are determined by fitting to the experimental stress–strain curve using the minimization of the relative error or the absolute difference. The degree of the constitutive model can be chosen depending on the complexity of the experimental curve. Table 3 summarizes the lowest average error obtained for each model and for different strain rates. For each strain rate, the constitutive models are ordered according to the lowest average error.

From Table 3, it is possible to identify the models that best characterizes the hyperelastic behaviour of the tested specimens. In this case, the Yeoh model is what describes the overall behaviour of the material for 1, 5 and 10 mm/min strain rates, while the Ogden model gave better performance for a strain rate of 2 mm/min. It should be pointed out that the results are only based on the stress–strain curve measured at the boundaries and not at the central region of the specimen.

**Table 3.** Models with the lowest average error.

1 mm/min	2 mm/min	5 mm/min	10 mm/min
Yeoh 2 (11.16%)	Ogden 2 (10.49%)	Yeoh 3 (9.48%)	Yeoh 2 (6.03%)
Ogden 2 (19.52%)	M.-Rivlin 3 (17.28%)	M.-Rivlin 3 (15.64%)	Ogden 2 (9.07%)
M.-Rivlin 3 (41.98%)	Yeoh 3 (18.20%)	Ogden 2 (34.86%)	M.-Rivlin 3 (21.93%)

The displacement fields in the central region obtained with numerical simulations using strain rates of 1 mm/min and 10 mm/min are shown in Figure 10. These feature for the same direction, a very similar distribution of the displacement field, varying only in amplitude.

In order to validate the numerical simulation, the profiles taken at the same central region were compared with experimentally measured profiles. In Figure 11, the numerical (FEM) and the experimental (DIC) profiles of the displacement along the X and Y directions for the strain rates of 1 mm/min and 10 mm/min are shown.

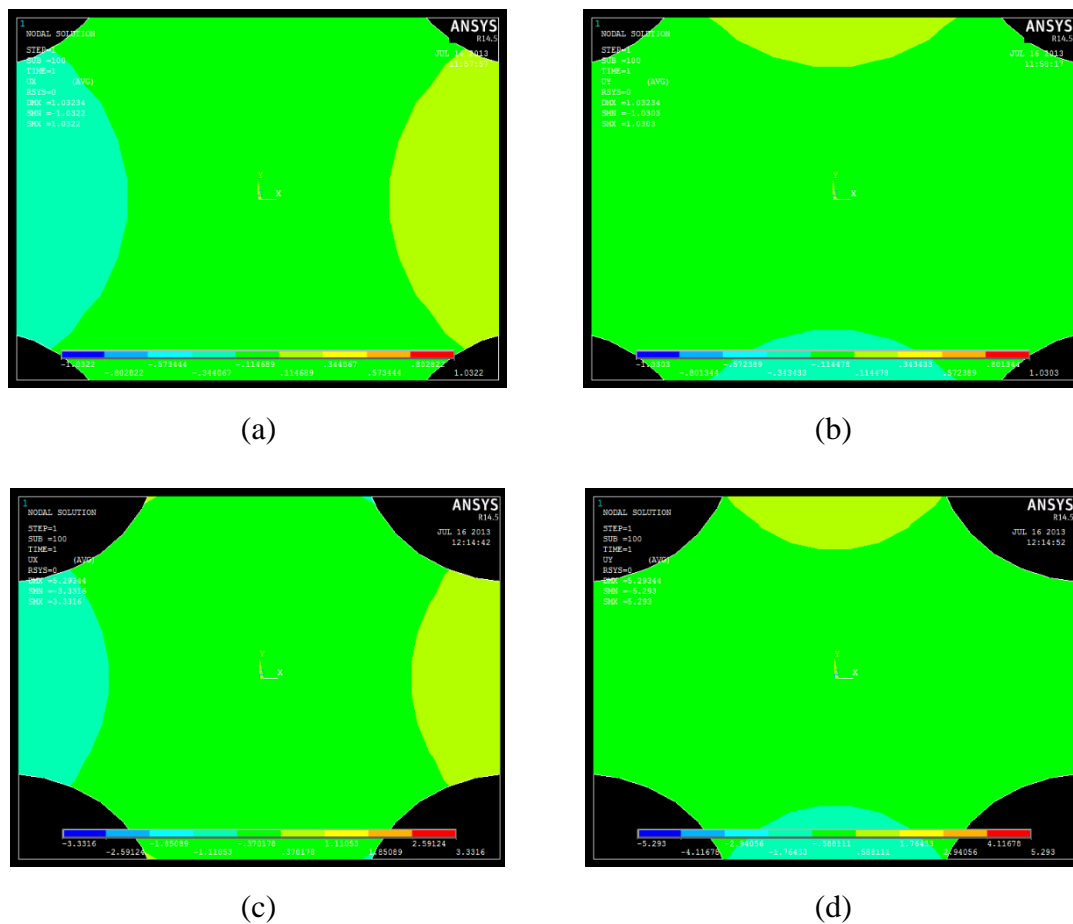


**Figure 10.** Displacement fields obtained by numerical simulation for a strain rate of 1 mm/min in the (a) X direction and (b) Y direction and a strain rate of 10 mm/min in the (c) X direction and (d) Y direction.

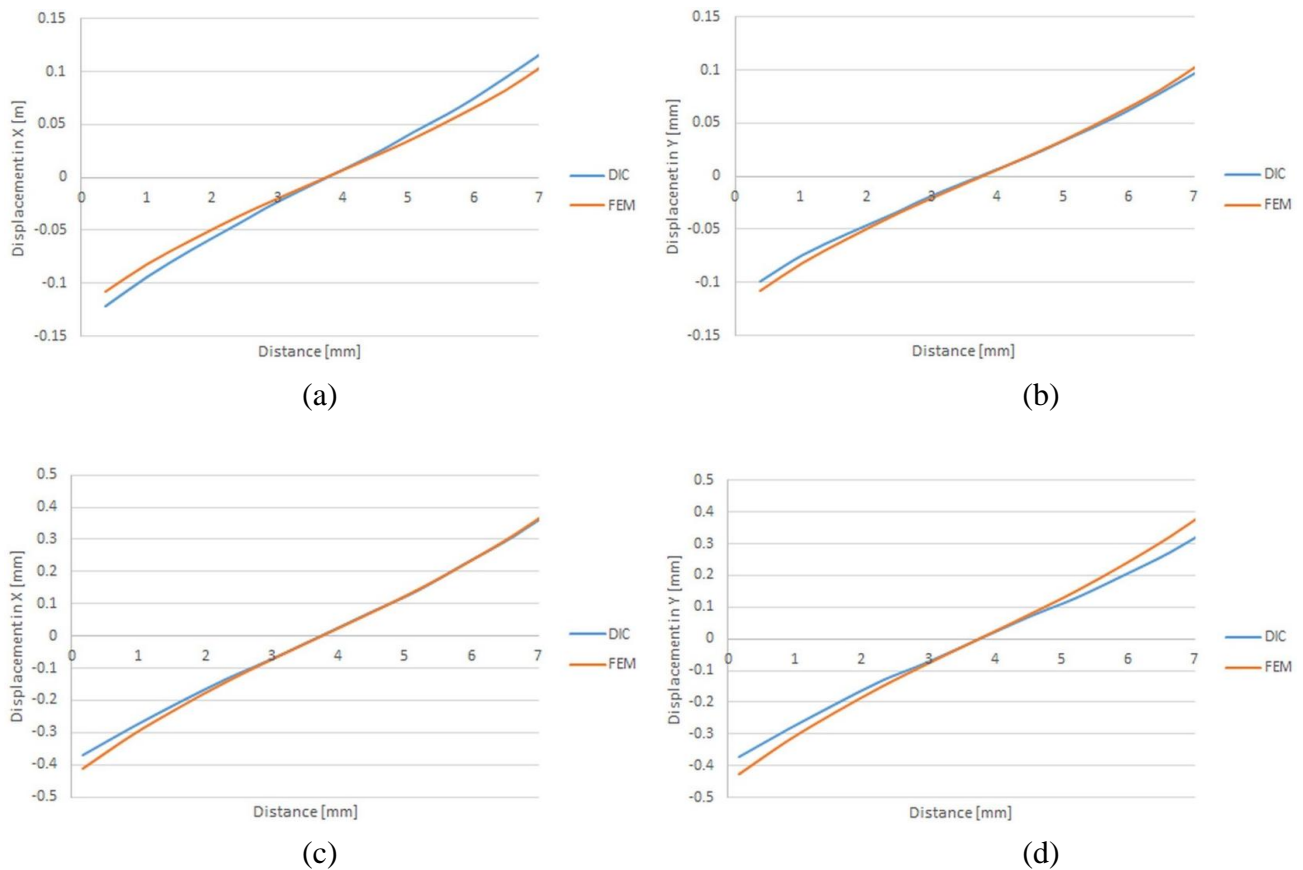


**Figure 11.** The experimental (DIC) and numerical (FEM) profiles of the displacement for a strain rate of 1 mm/min in the (a) X direction and (b) Y direction and a strain rate of 10 mm/min in the (c) X direction and (d) Y direction.

A detailed analysis of displacements reveals that, globally, there is a difference in the values at the region nearest the front of the grips. This can be explained by the average error in the hyperelastic constitutive models implemented in ANSYS.

In order to make comparative analysis simpler, the average error of the difference of displacement profiles for both directions is presented in Table 4.

Although there are significant average error differences between the experimental and numerical displacements, their values are acceptable for this kind of material.

**Table 4.** The average error between the experimental and numerical displacement profiles.

1 mm/min	2 mm/min	5 mm/min	10 mm/min
19.64%	17.60%	9.12%	8.06%

From the analysis of the average errors of the constitutive models, Table 3, and the displacement profiles, Table 4, it is possible to establish a direct relationship between the two values. Thus, one can conclude that the representativeness of the numerical model is strongly dependent on the constitutive model used to reproduce the experimental stress–strain curve. One should mention that the experimental curves are obtained based on measurements from the grips and represent the overall

behaviour of the material. This fact may also explain some of the deviations observed between the displacement field profiles.

## 5. Conclusions

The DIC technique was shown to be well suited for the measurement of displacement fields on hyperelastic materials. Given the high magnitude of displacements, the technique was capable of following the speckle pattern throughout the biaxial tensile tests, thus, allowing the measurement of large amplitude displacements.

In the biaxial experimental tests showed that displacements on the cruciform specimen are not symmetric and the values are different between orthogonal directions. The profiles of displacement along the X and Y directions presented an almost linear distribution.

The numerical simulation was carried out with different constitutive models of the material; the Ogden and Yeoh models presented the lowest average error. However, these models do not fully characterize the hyperelastic behaviour of the tested specimens, since some deviations between the model and the experimental stress–strain curves were observed. This led to a shift of numerical simulation displacements. Based on the average error analysis of the constitutive model and of the displacement profiles, it was possible to establish a direct relationship. Based on this, it is possible to state that the quality of the numerical result is strongly dependent on how well the constitutive model can follow the experimental stress–strain curve.

## Conflict of interest

The authors declare no conflict of interest.

## References

1. Ophir J, Céspedes I, Ponnekanti H, et al. (1991) Elastography: A quantitative method for imaging the elasticity of biological tissues. *Ultrasonic Imaging* 13: 111–134.
2. Greenleaf J, Fatemi M, Insana M (2003) Selected methods for imaging elastic properties of biological tissues. *Annu Rev Biomed Eng* 5: 57–78.
3. Choi D (2016) Mechanical characterization of biological tissues: Experimental methods based on mathematical modeling. *Biomed Eng Lett* 6: 181–195.
4. Bronzino JD (2000) *Biomedical Engineering Handbook*, 2 Eds., Florida: CRC Press LLC.
5. Enderle JD, Blanchard SM, Bronzino JD (2005) *Introduction to biomedical engineering*, 2 Eds., Oxford: Elsevier Academic Press.
6. Holzapfel GA (2000) *Nonlinear Solid Mechanics: A Continuum Approach for Engineering*, West Sussex: John Wiley & Sons Ltd.
7. Besson J, Cailletaud G, Chaboche J, et al. (2010) *Non-Linear Mechanics of Materials*, London: Springer Science & Business Media.
8. Yannas I, Burke J (1980) Design of an artificial skin. I. Basic design principles. *J Biomed Mater Res* 14: 65–81.
9. Tompkins R, Burke J (1990) Progress in burn treatment and the use of artificial skin. *World J Surg* 14: 819–824.

10. Sopyan I, Mel M, Ramesh S, et al. (2007) Porous hydroxyapatite for artificial bone applications. *Sci Technol Adv Mat* 8: 116–123.
11. Afonso J, Martins P, Girão M, et al. (2008) Mechanical properties of polypropylene mesh used in pelvic floor repair. *Int Urogynecol J* 19: 375–380.
12. Pinho D, Bento D, Ribeiro J, et al. (2015) An In Vitro Experimental Evaluation of the Displacement Field in an Intracranial Aneurysm Model, In: Flores P, Viadero F, *New Trends in Mechanism and Machine Science: From Fundamentals to Industrial Applications*, Springer, 261–268.
13. Bernardi L, Hopf R, Ferrari A, et al. (2017) On the large strain deformation behavior of silicone-based elastomers for biomedical applications. *Polym Test* 58: 189–198.
14. Aziz T, Waters M, Jagger R (2003) Analysis of the properties of silicone rubber maxillofacial prosthetic materials. *J Dent* 31: 67–74.
15. Gerratt A, Michaud H, Lacour S (2015) Elastomeric electronic skin for prosthetic tactile sensation. *Adv Funct Mater* 25: 2287–2295.
16. Yu YS, Zhao YP (2009) Deformation of PDMS membrane and microcantilever by a water droplet: Comparison between Mooney–Rivlin and linear elastic constitutive models. *J Colloid Interf Sci* 332: 467–476.
17. Yu YS, Yang Z, Zhao YP (2008) Role of vertical component of surface tension of the droplet on the elastic deformation of PDMS membrane. *J Adhes Sci Technol* 22: 687–698.
18. Martins P, Peña E, Calvo B, et al. (2010) Prediction of nonlinear elastic behaviour of vaginal tissue: experimental results and model formulation. *Comput Method Biomec* 13: 327–337.
19. Bakar MSA, Cheng MHW, Tang SM, et al. (2003) Tensile properties, tension-tension fatigue and biological response of polyetheretherketone-hydroxyapatite composites for load-bearing orthopedic implants. *Biomaterials* 24: 2245–2250.
20. Wang RZ, Weiner S (1997) Strain–structure relations in human teeth using Moiré fringes. *J Biomech* 31: 135–141.
21. Zaslansky P, Shahar R, Friesem AA, et al. (2006) Relations between shape, materials properties, and function in biological materials using laser speckle interferometry: in situ tooth deformation. *Adv Funct Mater* 16: 1925–1936.
22. Sujatha NU, Murukeshan VM (2004) Nondestructive inspection of tissue/tissue like phantom curved surfaces using digital speckle shearography. *Opt Eng* 43: 3055–3060.
23. Zhang DS, Arola DD (2004) Applications of digital image correlation to biological tissues. *J Biomed Opt* 9: 691–699.
24. Rodrigues R, Pinho D, Bento D, et al. (2016) Wall Expansion assessment of an intracranial aneurysm model by a 3D Digital Image Correlation system. *Measurement* 88: 262–270.
25. Ribeiro J, Fernandes CS, Lima R (2017) Numerical Simulation of Hyperelastic Behaviour in Aneurysm Models, In: Tavares J, Natal Jorge R, *Lecture Notes in Computational Vision and Biomechanics*, Springer, 937–944.
26. Bischoff JE, Arruda EM, Grosh K (2000) Finite element modeling of human skin using an isotropic, nonlinear elastic constitutive model. *J Biomech* 33: 645–652.
27. Ribeiro J, Lopes H, Martins P (2017) A hybrid method to characterize the mechanical behaviour of biological hyperelastic tissues. *Comput Method Biomech Biomed Eng Imag Visual* 5: 157–164.

28. Sutton MA, Orteu JJ, Scheier HW (2009) *Image Correlation for Shape, Motion and Deformation Measurements: Basic Concepts, Theory and Applications*, Springer Science & Business Media.
29. Nunes LCS (2011) Mechanical characterization of hyperelastic polydimethylsiloxane by simple shear test. *Mat Sci Eng A-Struct* 528: 1799–1804.
30. Cardoso C, Fernandes C, Lima R, et al. (2018) Biomechanical analysis of PDMS channels using different hyperelastic numerical constitutive models. *Mech Res Commun* 90: 26–33.
31. Madenci E, Guven I (2015) *The Finite Element Method and Applications in Engineering Using ANSYS®*, New York: Springer.



AIMS Press

© 2019 the Author(s), licensee AIMS Press. This is an open access article distributed under the terms of the Creative Commons Attribution License (<http://creativecommons.org/licenses/by/4.0>)